Fill-factor improvement of Si CMOS single-photon avalanche diode detector arrays by integration of diffractive microlens arrays

Giuseppe Intermite,[1*] Aongus McCarthy,[1] Ryan E. Warburton,[1] Ximing Ren,[1] Federica Villa,[2] Rudi Lussana,[2] Andrew J. Waddie,[1] Mohammad R. Taghizadeh,[1] Alberto Tosi,[2] Franco Zappa,[2] and Gerald S. Buller[1]

[1]Institute of Photonics and Quantum Sciences, and Scottish Universities Physics Alliance (SUPA, School of Engineering and Physical Sciences, Heriot-Watt University, EH14 4AS, United Kingdom
[2]Politecnico di Milano, Dipartimento di Elettronica, Informazione e Bioingegneria, Piazza Leonardo Da Vinci 32, I-20133 Milano, Italy
[*]gi23@hw.ac.uk

Abstract: Single-photon avalanche diode (SPAD) detector arrays generally suffer from having a low fill-factor, in which the photo-sensitive area of each pixel is small compared to the overall area of the pixel. This paper describes the integration of different configurations of high efficiency diffractive optical microlens arrays onto a 32×32 SPAD array, fabricated using a 0.35 µm CMOS technology process. The characterization of SPAD arrays with integrated microlens arrays is reported over the spectral range of 500-900 nm, and a range of f-numbers from f/2 to f/22. We report an average concentration factor of 15 measured for the entire SPAD array with integrated microlens array. The integrated SPAD and microlens array demonstrated a very high uniformity in overall efficiency.

References and links

1. G. Gariepy, N. Krstajić, R. Henderson, C. Li, R. R. Thomson, G. S. Buller, B. Heshmat, R. Raskar, J. Leach, and D. Faccio, "Erratum: Single-photon sensitive light-in-flight imaging," Nat. Commun. **6**, 6408 (2015).
2. A. McCarthy, X. Ren, A. Della Frera, N. R. Gemmell, N. J. Krichel, C. Scarcella, A. Ruggeri, A. Tosi, and G. S. Buller, "Kilometer-range depth imaging at 1,550 nm wavelength using an InGaAs/InP single-photon avalanche diode detector," Opt. Express **21**(19), 22098–22113 (2013).
3. A. M. Wallace, A. McCarthy, C. J. Nichol, X. Ren, S. Morak, D. Martinez-Ramirez, I. H. Woodhouse, and G. S. Buller, "Design and Evaluation of Multispectral LiDAR for the Recovery of Arboreal Parameters," IEEE Trans. Geosci. Rem. Sens. **52**(8), 4942–4954 (2014).
4. A. McCarthy, R. J. Collins, N. J. Krichel, V. Fernández, A. M. Wallace, and G. S. Buller, "Long-range time-of-flight scanning sensor based on high-speed time-correlated single-photon counting," Appl. Opt. **48**(32), 6241–6251 (2009).
5. D.-U. Li, J. Arlt, J. Richardson, R. Walker, A. Buts, D. Stoppa, E. Charbon, and R. Henderson, "Real-time fluorescence lifetime imaging system with a 32 x 32 0.13micron CMOS low dark-count single-photon avalanche diode array," Opt. Express **18**(10), 10257–10269 (2010).
6. W. Becker, *Advanced Time-Correlated Single Photon Counting Techniques*, Springer Series in Chemical Physics (Springer, 2005), Vol. 81.
7. G. S. Buller and R. J. Collins, "Single-photon generation and detection," Meas. Sci. Technol. **21**(1), 012002 (2010).
8. R. E. Warburton, G. Intermite, M. Myronov, P. Allred, D. R. Leadley, K. Gallacher, D. J. Paul, N. J. Pilgrim, L. J. M. Lever, Z. Ikonic, R. W. Kelsall, E. Huante-Ceron, A. P. Knights, and G. S. Buller, "Ge-on-Si Single-Photon Avalanche Diode Detectors: Design, Modeling, Fabrication, and Characterization at Wavelengths 1310 and 1550 nm," IEEE Trans. Electron. Dev. **60**(11), 3807–3813 (2013).
9. F. Zappa, S. Tisa, A. Tosi, and S. Cova, "Principles and features of single-photon avalanche diode arrays," Sens. Actuat. Phys. **140**(1), 103–112 (2007).
10. C. S. Menoni, "Breakthroughs in Photonics 2010," IEEE Photonics J. **3**, 241–336 (2011).

11. S. Cova, M. Ghioni, A. Lacaita, C. Samori, and F. Zappa, "Avalanche photodiodes and quenching circuits for single-photon detection," Appl. Opt. **35**(12), 1956–1976 (1996).
12. C. Scarcella, A. Tosi, F. Villa, S. Tisa, and F. Zappa, "Low-noise low-jitter 32-pixels CMOS single-photon avalanche diodes array for single-photon counting from 300 nm to 900 nm," Rev. Sci. Instrum. **84**(12), 123112 (2013).
13. D. Bronzi, F. Villa, S. Tisa, A. Tosi, F. Zappa, D. Durini, S. Weyers, and W. Brockherde, "100000 Frames/s 64 x 32 Single-Photon Detector Array for 2-D Imaging and 3-D Ranging," IEEE J. Sel. Top. Quantum Electron. **20**(6), 354–363 (2014).
14. C. Niclass, C. Favi, T. Kluter, M. Gersbach, and E. Charbon, "A 128x128 Single-Photon Image Sensor with Column-Level 10-bit Time-to-Digital Converter Array," J. Solid-State Circuits **43**(12), 2977–2989 (2008).
15. M. Gersbach, Y. Maruyama, R. Trimananda, M. W. Fishburn, D. Stoppa, J. A. Richardson, R. Walker, R. Henderson, and E. Charbon, "A Time-Resolved, Low-Noise Single-Photon Image Sensor Fabricated in Deep-Submicron CMOS Technology," IEEE J. Solid-State Circuits **47**(6), 1394–1407 (2012).
16. F. Villa, R. Lussana, D. Bronzi, S. Tisa, A. Tosi, F. Zappa, A. Dalla Mora, D. Contini, D. Durini, S. Weyers, and W. Brockherde, "CMOS Imager With 1024 SPADs and TDCs for Single-Photon Timing and 3-D Time-of-Flight," IEEE J. Sel. Top. Quantum Electron. **20**(6), 364–373 (2014).
17. D. Bronzi, F. Villa, S. Tisa, A. Tosi, and F. Zappa, "SPAD Detectors and Imagers: Figures of merit for Photon-counting and Photon-timing Applications," IEEE Sens. J. in press.
18. F. Villa, B. Markovic, S. Bellisai, D. Bronzi, A. Tosi, F. Zappa, S. Tisa, D. Durini, S. Weyers, U. Paschen, and W. Brockherde, "SPAD Smart Pixel for Time-of-Flight and Time-Correlated Single-Photon Counting Measurements," IEEE Photonics J. **4**(3), 795–804 (2012).
19. S. Donati, G. Martini, and M. Norgia, "Microconcentrators to recover fill-factor in image photodetectors with pixel on-board processing circuits," Opt. Express **15**(26), 18066–18075 (2007).
20. S. Donati, G. Martini, and E. Randone, "Improving Photodetector Performance by Means of Microoptics Concentrators," J. Lightwave Technol. **29**(5), 661–665 (2011).
21. S. Donati, E. Randone, M. Fathi, J.-H. Lee, and E. Charbon, "Uniformity of concentration factor and back focal length in molded polymer microlens arrays," in *Conference on Lasers and Electro-Optics (CLEO) and Quantum Electronics and Laser Science Conference (QELS),* (OSA / CLEO / QELS, 2010).
22. J. M. Pavia, M. Wolf, and E. Charbon, "Measurement and modeling of microlenses fabricated on single-photon avalanche diode arrays for fill factor recovery," Opt. Express **22**(4), 4202–4213 (2014).
23. F. Villa, D. Bronzi, Y. Zou, C. Scarcella, G. Boso, S. Tisa, A. Tosi, F. Zappa, D. Durini, S. Weyers, U. Paschen, and W. Brockherde, "CMOS SPADs with up to 500 μm diameter and 55% detection efficiency at 420 nm," J. Mod. Opt. **61**(2), 102–115 (2014).
24. R. Lussana, F. Villa, A. D. Mora, D. Contini, A. Tosi, and F. Zappa, "Enhanced single-photon time-of-flight 3D ranging," Opt. Express **23**(19), 24962–24973 (2015).
25. B. C. Kress and P. Meyrueis, *Applied Digital Optics: From Micro-Optics to Nanophotonics* (John Wiley & Sons, 2009).
26. J. Jahns and S. J. Walker, "Two-dimensional array of diffractive microlenses fabricated by thin film deposition," Appl. Opt. **29**(7), 931–936 (1990).
27. M. R. Taghizadeh, P. Blair, B. Layet, I. M. Barton, A. J. Waddie, and N. Ross, "Design and fabrication of diffractive optical elements," Microelectron. Eng. **34**(3-4), 219–242 (1997).
28. H. P. Herzig, *Micro-Optics: Elements, Systems And Applications* (CRC Press, 1997).
29. J. W. Goodman, *Introduction to Fourier Optics,* 2nd Ed., (McGraw-Hill, 1996).

1. Introduction

Picosecond-resolution detection of single-photons in the visible and near-infrared (NIR) spectral range below a wavelength of 1 μm is required in many photon-starved applications such as time-of-flight ranging and imaging and time-resolved biomedical science (e.g. fluorescence lifetime imaging, and positron emission tomography) [1–5].

In this spectral range, detection of low–light level optical signals with picosecond timing resolution can be achieved using time-correlated single photon counting approaches [6], where a variety of single-photon detector options are available. Single-photon detectors such as photomultiplier tubes (PMTs), microchannel plates, superconducting single-photon detectors, and single-photon avalanche diode (SPAD) detectors have been developed to satisfy requirements in terms of single-photon sensitivity and picosecond timing resolution [7,8]. Amongst these various options, low-noise Si SPADs are now a commercially available technology and are preferred because of their intrinsic advantages of low electrical power consumption, miniature size, low bias voltages, near room temperature operation, reduced magnetic field susceptibility, high reliability, and potentially low cost [9–11].

Si SPAD detectors can be classified into two distinct groups: those fabricated using customized processing techniques and those fabricated using CMOS compatible approaches. The former devices are based on tailored processing with the aim of obtaining the best performance from the photodiode when operated in Geiger-mode. The latter devices rely on standard CMOS fabrication processes which offer significant advantages in terms of the routine on-chip integration with the electronics required for photon-counting and photon-timing techniques. From the early 2000s, several research groups have explored the design of a monolithically integrated single-photon imaging systems in high-voltage (HV) and standard deep-sub-micron (DSM) CMOS technologies [12–16]. This efficient integration allows the possibility of fabrication of two-dimensional SPAD-based focal plane arrays. Scaling down of the CMOS process may offer some advantages in reduced jitter through device miniaturization, however it usually results in higher dark count rate (DCR) and it may not necessarily result in increased single-photon detection efficiency (SPDE) compared with custom processed SPADs [16,17]. In addition, when in-pixel circuitry is included as in a CMOS Si SPAD array, we can refer to a pixel as a *smart* pixel [18]. Inevitably the in-pixel circuitry compromises the available proportion of detector photo-sensitive area, and we need to consider the issue of geometric fill-factor which is the ratio of photo-sensitive area to total pixel area. A reduction in fill-factor causes a further deterioration of the effective SPDE, since a larger fraction of incident photons cannot be detected.

A number of approaches have been attempted, including the use of non-imaging concentrators such as reflective-based structures [19], however these are difficult to fabricate on the scale required. Other approaches utilizing molded refractive microlens have been used [20,21] and large improvements in maximum fill-factor were reported for arrays, which compared well with the theoretical maximum value predicted over parts of the detector array. More recently, Mata Pavia et al [22] reported arrays of refractive microlens arrays integrated on SPAD arrays, which had concentration factors in the range of 10 at higher f-numbers.

In this paper, we report high fill-factor which was achieved as a result of integrating diffractive microlens arrays with 32 × 32 SPAD arrays with 3.14% fill-factor. The design and integration of two different sets of 32 × 32 plano-convex infinite and finite conjugate microlenses is described. To the best of our knowledge, this is the first report of a full characterization of SPAD arrays with integrated microlenses over a large spectral range (500-900 nm), with the illumination f-number varying from f/2 to f/22, and with full pixel uniformity data measured across the entire array. Measurements of the concentration factor (CF) and spatial uniformity are performed by using a double telecentric imaging system. To the best of our knowledge, we report the highest value of the concentration factor for a full microlens array integrated with a SPAD array, with the best reported value for uniformity across the whole detector array after integration of the microlens and SPAD arrays.

2. HV-CMOS Si SPAD Array

The 32 × 32 Si CMOS SPAD detector arrays used in this research work were developed under the European Commission funded project MiSPIA (Microelectronic Single-Photon 3D Imaging Array for low-light high-speed Safety and Security Applications). These arrays were fabricated by using a 0.35 μm HV-CMOS technology process at the Fraunhofer foundry IMS [16]. The 32 × 32 array was composed of square 150 μm × 150 μm dimensioned pixels, with each pixel containing a 30 μm active area diameter SPAD detector and all associated circuitry for detector quenching, photon counting and photon timing. A schematic block diagram of the smart pixel and a microscope image of a section of the SPAD array are illustrated in Fig. 1(a) and 1(b). These smart pixel dimensions resulted in a fill-factor of 3.14% when not used in conjunction with microlenses.
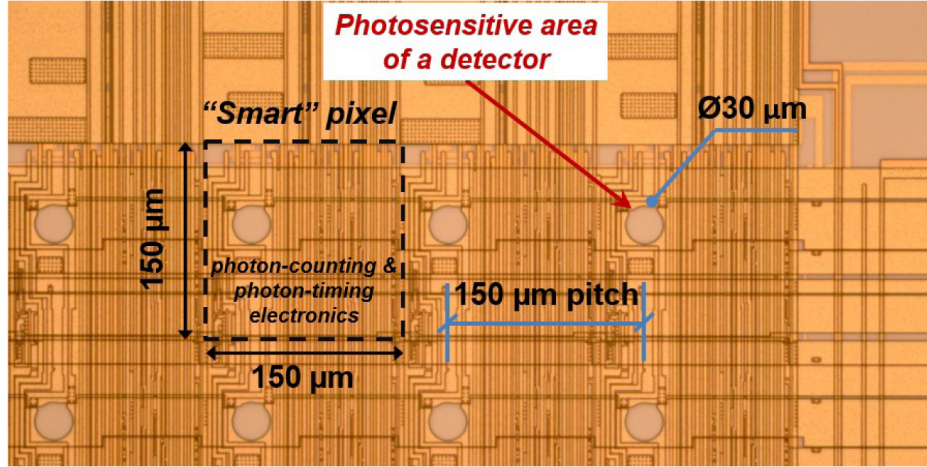
Fig. 1. (a) Block diagram of the "smart" pixel, with overall dimensions of 150 μm × 150 μm, employing a SPAD with active area diameter of 30 μm. This corresponds to a fill-factor of 3.14% for the chip with no microlens. (b) Microscope image of a section of the Si CMOS SPAD array with no integrated microlens.

The single-photon detection performance of the 30 μm diameter SPADs are reported in detail in [23]. These devices demonstrated a maximum SPDE of 55% at a wavelength of 450 nm, which reduced to 20% at 650 nm wavelength and 5% at a wavelength of 850 nm. Removing the small proportion of hot pixels (see below), the average DCR at room temperature was 120 counts/s at 6V excess bias, while the timing jitter at a wavelength of 450 nm was 85 ps full-width half-maximum (FWHM).

The in-pixel electronics included a quenching circuit with active reset for fast avalanche sensing and quenching, pulse shaping electronics for proper synchronization, a 10 bit time to digital converter (TDC), a 6 bit counter, and an 8 bit memory register. The array was designed to work in two modes of operation: photon-counting and photon-timing. The photon-counting mode was used to perform the characterization measurements reported in this paper, with this mode being used to count the number of photon events within a pre-determined frame duration, that can be varied between 50 ns to 500 ms [18]. In this photon-counting mode, either a photon-initiated event, or a dark count, triggers the avalanche process by producing a macroscopic signal which is then sensed by the quenching circuit. The avalanche is quenched and the counter is incremented. After a well-defined 50 ns hold-off time, during which photons cannot be detected, the SPAD is reset back to its original quiescent state, ready to detect other photons. These operations are performed throughout the duration of a frame and all pixels work independently. The beginning of a frame is marked by sequence of the Stop and Start signals, which are applied in parallel to all pixels of the array. Therefore all accumulated counts are frozen at the same time and are stored into the 1024 in-pixel registers. Data read-out is carried out using a row-column access scheme. The limit for the maximum achievable frame-rate (i.e. the minimum frame duration) is given by the time necessary to read the whole array. More details on smart pixel architecture and operation can be found in [19,24].

3. Diffractive microlens arrays design, performance and integration

The phase function of a microlens can be implemented as either a refractive component, where the lens power is provided by means of a continuous curvature of the surface, or as a diffractive element, where the lens power is produced by means of a spatially-varying rotationally-symmetric blazed grating structure. The refractive microlens approach potentially offers a greater spectral bandwidth at the expense of incomplete filling of the square pixel

area, especially when fabricated using the resist reflow technique [25] which is the most straightforward and reliable approach for this work. Diffractive microlenses, which are designed for a single wavelength of operation and give reduced spectral bandwidth (typically on the order of 100 nm-200 nm), do allow a 100% fill-factor and were used in this work for precisely that reason. The microlenses were fabricated using Fresnel-like grooves and the lens surface was approximated by a modulo 2π zone plate representation, resulting in a fill-factor of the available area of ~100% (i.e. no dead zone between microlenses) for a square pixel. The widths of the modulo 2π, (i.e. the edges of the zones where there is a 2π step) were determined from the following equations:

$$M = (2m+1)dm$$
$$N = M + dm$$
$$r_i = \sqrt{2M\lambda f + M^2\lambda^2}$$
$$r_o = \sqrt{2N\lambda f + N^2\lambda^2}$$

(1)

where m is the zone number (from 0 at the centre of the lens), dm is 0.5 for the 2π zones (i.e. the zones which end with a 2π phase jump), λ the designed wavelength, f the focal length r_i and r_0 are the inner and outer radius of the m-th zone, respectively. All the lens power of the diffractive lenses is provided by the circular blazed grating structure (i.e. there is no curvature of the substrate to provide any refractive power).

With the diffractive microlenses used in this paper a total of 75-85% of the incident light at the design wavelength is directed into the diffraction-limited central focal spot. The loss in overall focussing efficiency is due to the finite number of discrete phase levels used to represent the rotationally symmetric blazed grating structure [26] and is shown in Fig. 2. Diffractive microlenses belong to the category of digital diffractive optics where their performance is determined numerically by the solution of the Helmholtz equation and fabricated through well-established lithographic techniques using binary amplitude masks, in a similar manner to VLSI electronics. The diffractive microlens has a staircase-like phase profile, and can be approximated by power-of-two (N) discrete phase levels which are fabricated through application of $\log_2(N)$ binary amplitude masks in sequence [27]. In this particular case, the fabricated diffractive microlens arrays consisted of 16 phase levels, and hence four successive binary masks ($16 = 2^4$) were required to be generated. These four masks were then used in multilevel photolithography to generate the 16 phase levels.

Although, diffractive microlenses are sensitive to changes in operational wavelength and exhibit a wavelength dependent focal length [28], they can work over a wider range of wavelengths. The microlens arrays used in this research were designed to operate with maximum efficiency at a wavelength of 808 nm. A calculation of the overall focussing efficiency of the lens was made using conventional grating theory [29]. The focussing efficiency is the fraction of light focussed into the diffraction limited spot. A simulation of the coupling efficiency (and hence the theoretical CF), as a function of the operational wavelength for the designed diffractive microlens was performed using custom made software (which was a developed implementation of the Angular Spectrum of Plane Waves method [29]). The comparison between the grating theory calculation and the more complete ASPW simulation shows the effect of higher order foci as shown in Fig. 2. Here, the overall coupling efficiency is defined as the percentage of the incident light on the microlens being concentrated within a 30 μm diameter circle on a pre-determined plane which is placed a fixed distance from the microlens. In this case the plane is fixed as being the rear surface of the microlens substrate where the detector array will be positioned after integration. The CF is calculated by dividing the coupling efficiency by the percentage fill-factor of the unmodified SPAD array. The microlens aperture is matched exactly to the dimensions of the detector pixel, being square of side 150 μm. In principle, a diffractive lens can achieve 100% coupling

efficiency, however quantization errors resulting from the approximation of a continuous phase surface by a finite number of discrete phase levels mean that the maximum efficiency, in this case, is approximately 80%. We are working on improving this maximum efficiency by using a larger number of phase levels and reducing the minimum feature size, although the fabrication process becomes more challenging.
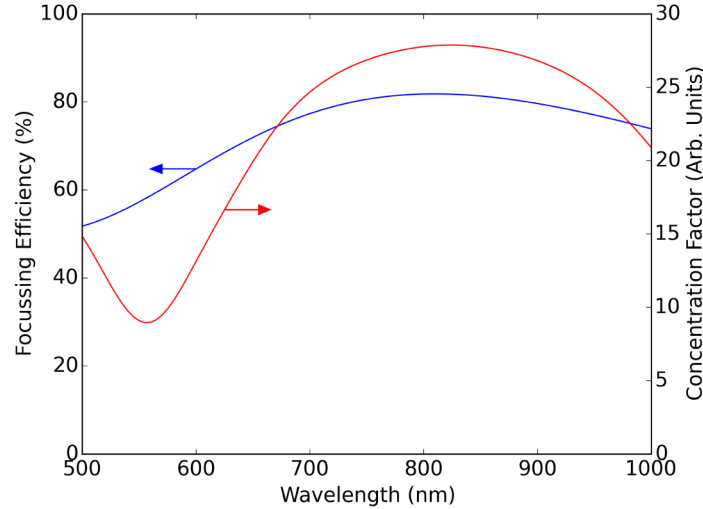

Fig. 2. Overall coupling efficiency (blue) and theoretical CF (red) versus wavelength for the designed diffractive microlens in infinite conjugate configuration. Microlenses were designed to work at a wavelength of 808 nm, but can produce a focal spot within the SPAD active area over a significant range of wavelength.

Due to the fabrication limitations on the minimum attainable feature size (~1.8 μm), the f-number of the microlenses was constrained to be greater than f/2.9 in order to ensure a 100% fill-factor. To improve the mechanical handling capabilities of the microlens arrays, it was decided to use fused silica substrates with thicknesses of between 0.5 and 1.0 mm. Two different designs of diffractive microlenses were selected for fabrication– one design was for operation in an infinite conjugate arrangement, the other for a finite conjugate configuration. The "infinite conjugate" configuration were designed with the focal length exactly equal to the thickness of the substrate, so that light parallel to the optic axis would be focussed at the plane of the back of the substrate, which is directly bonded onto the plane of the SPAD array. The "finite conjugate" configuration microlenses were designed to concentrate light from an object plane placed at a short distance from the microlens array onto the back surface of the substrate. In both configurations, the imaging of the scene is performed by an external bulk lens, and the microlens arrays are used to concentrate light from this image plane onto the small SPAD active areas. This means that the individual microlens performs the function of an optical concentrator, transferring light from a pixel within a larger image onto the active area of the corresponding detector active area. A schematic representation of both microlenses is shown in Fig. 3(a) and 3(b).

The infinite conjugate microlens array was fabricated on a 1 mm thick substrate and this corresponds to a lens with an f-number of f/4.6 (for an equivalent lens designed for operation in free space). This lens configuration allowed the performance of the fabricated lenses (e.g. focal length, optical efficiency, and spot sizes) to be readily assessed so that the microlens design and fabrication process could be refined appropriately.
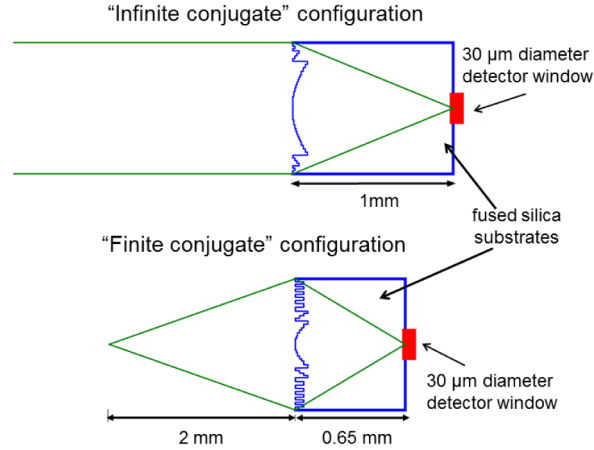
Fig. 3. Schematic representation of the designed microlenses: (a) infinite conjugate microlenses were designed to concentrate light from an object placed at infinity; and (b) finite conjugate microlenses were designed to concentrate light from an image plane at a distance of 2 mm in front of the microlens array onto the detector.

The focal lengths of the infinite conjugate diffractive lens arrays were tested using a 780 nm wavelength source, due to the lack of availability of a 808 nm wavelength source at that time. For the f/4.6 diffractive microlens, the focal length at a wavelength of 808 nm was designed to be 0.690 mm, while the calculated and measured focal length (at a wavelength of 780 nm) was equal to 0.715 mm and 0.703 mm ± 0.01 mm, which corresponded to a focal length in fused silica of 1.022 ± 0.014 mm. At the same wavelength, the diffraction limited spot diameter ($1/e^2$ width) predicted by theory was 9 μm, while the estimated focal spot size was 7.6 μm ± 2 μm. Figure 4 shows an image of a part of the 32 × 32 diffractive microlens array designed to operate at a wavelength of 808 nm (left), and the focal spot size which was obtained by magnified image of the focal plane on a CCD camera (right).
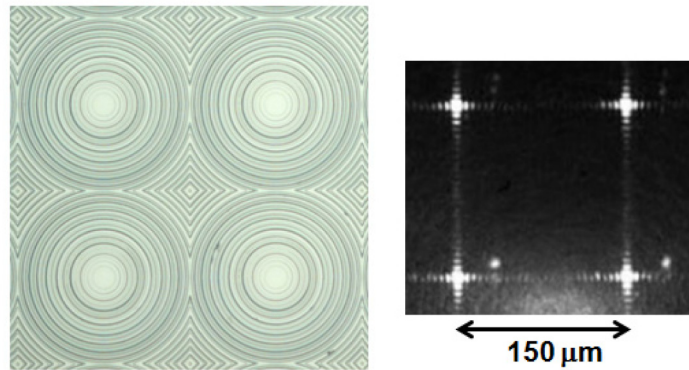

Fig. 4. (left) An optical microscope image showing part of 32 × 32 infinite conjugate microlens array designed to operate at a wavelength of 808 nm. (right) magnified image of the microlens focal plane recorded on a CCD camera. The microlenses, and focused spots, are on 150 μm square pitch.

The finite conjugate lens array was fabricated on a 0.650 mm thick substrate and had a design focal length of approximately 0.32 mm or 0.465 mm in fused silica. This focal length was chosen so that in order to align the image plane with the detector array, the image plane formed by the external lens would need to be 2 mm in front of the lens. This meant that a

microlens magnification of −0.2 would concentrate a 150 μm × 150 μm square area of the image onto the 30 μm diameter active area of SPAD array.

The 32 × 32 microlens array substrates were approximately 5.6 mm × 5.6 mm in overall outer dimensions and were bonded to the top surface of the 9 mm × 9 mm SPAD array chips to form a single assembly. In order to perform this operation, three metal (chrome) alignment marks, or fiducials, were deposited on the microlens substrate, on the same surface as the microlens array. Matching metal fiducials were also included on the SPAD array chips during its fabrication. The microlens arrays and SPAD arrays were mounted (held in place with vacuum chucks) in a flip-chip bonder (Karl Suss FC6) which could achieve a bonding alignment with an accuracy of less than 5 μm across the entire detector array area. The fiducials on both the detector and microlens arrays were first aligned, the appropriate bonding parameters were then configured, and the bonding sequence was initiated. After a post-bond visual inspection of the fiducial alignment using a microscope, the wire bonding of the electrical connections to the SPAD array was then carried out, to permit photon-counting characterization of the integrated detector array.

4. Experimental characterization setup

The optical setup used for the characterization of the SPAD arrays integrated with the two different sets of diffractive microlenses arrays (described in section 3) is illustrated in Fig. 5.
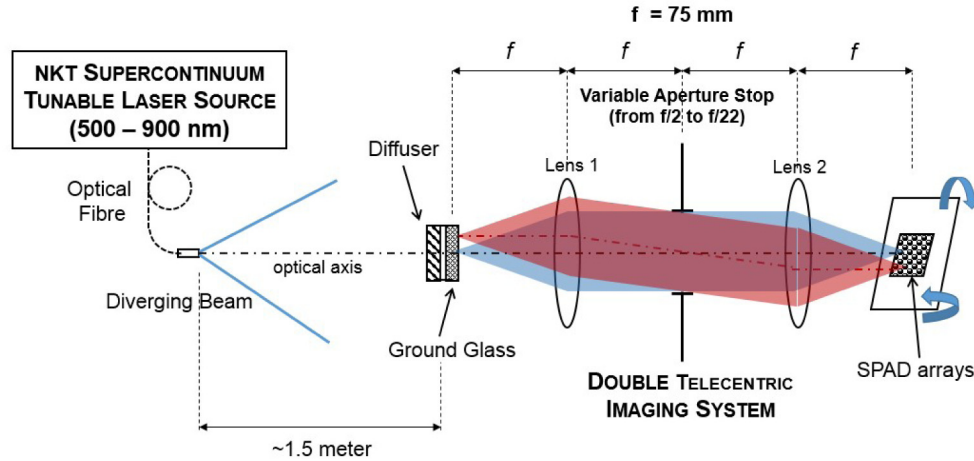

Fig. 5. Experimental setup used to evaluate the concentration factor at varying f-numbers (from f/2 to f/22 in one-stop increments) and different wavelengths between 500 nm and 900 nm. This setup was also used to evaluate the uniformity of SPAD arrays.

A NKT Supercontinuum laser source (SuperK Extreme EX-W6) was used as a source for the measurement of the CF and uniformity in the spectral range between 500 and 900 nm. The laser used an acousto-optic tunable filter (AOTF) for wavelength selection. Light coupled in a single-mode fibre (5 μm diameter core) then diverges upon exiting the fibre and propagates along the optical bench over a length of ~1.5 meters where the central part of the beam was incident on a diffuser. This diffuser ensured that the near-collimated light is diffused uniformly throughout a large cone angle (~50°). After the diffuser, a ground glass plate was inserted to act as the surface to be imaged onto the SPAD arrays by means of a customized double telecentric image system. The telecentric system offers advantages such as a constant magnification over a defined depth of field (the setup in Fig. 5 had a fixed magnification of 1:1), no perspective error, very low geometrical distortion, and highly uniform illumination. This system was composed of two identical 50 mm diameter achromatic doublet lenses (focal length, $f = 75$ mm), with an aperture stop placed at the common focal point. The three SPAD

detector arrays (namely the bare SPAD chip, the integrated SPAD array with infinite conjugate microlenses, and the integrated SPAD array with finite conjugate microlenses) were mounted, in turn, on a micrometer six-axis positioning stage which was placed at a distance f from the rear lens of the telecentric system. The SPAD arrays were aligned to be orthogonal to the optical axis of the double telecentric imaging system. For this purpose, a collimated reference beam was used to ensure that the incident light was normally incident on the SPAD array chip. The light level was restricted to the single-photon regime for measurements with all SPAD geometries, due to large losses incurred while using only a small proportion of the central part of the beam to ensure uniform illumination of the optical diffuser.

The optical setup illustrated in Fig. 5 was used to characterize the SPAD arrays, which had the integrated diffractive microlenses arrays, in terms of two main parameters: the CF and spatial uniformity. Measurements of both parameters were performed at different f-numbers (from f/2 to f/22 with one-stop increments), and different wavelengths between 500 nm and 900 nm. In addition, all the reported measurements were performed at room temperature and in dark conditions. The excess bias voltage on the SPAD arrays under test, with and without microlens arrays, was kept fixed at a value of 3 V.
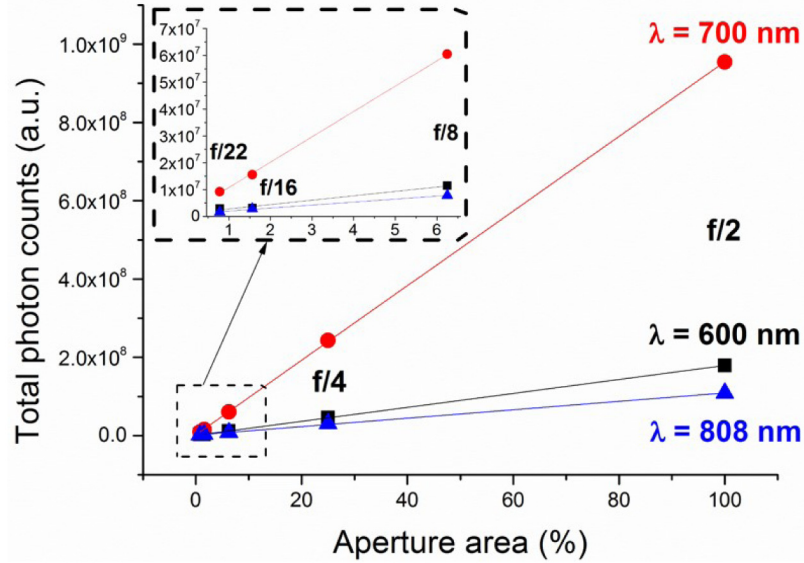

Fig. 6. Linearity test of the total photon counts collected from the SPAD array (without microlenses) as a function of the aperture area (f-number). This test was performed at a constant laser power and three different wavelengths, 600 nm (shown in black), 700 nm (red), and 808 nm (blue). Linear fitting is also shown. The inset in the figure also shows the linearity at the highest f-numbers, f/8, f/16, and f/22 respectively.

This optical system worked in a similar manner to a camera system, such that when the f-number is increased by one-stop, the light intensity at the camera sensor is halved, to provide a linear relationship between the f-number and the light intensity. Therefore, the robustness of the characterization setup was demonstrated by measuring this linear relationship between the total photon counts (light intensity) for the SPAD sensor without microlenses, as a function of the aperture area (f-number) between f/2 and f/22. The total number of counts for the SPAD array was obtained by firstly obtaining an image of the SPAD array under completely dark conditions, to provide a background estimate. The SPAD sensor was then illuminated with light at a specific wavelength to provide the signal estimate. Finally, the background was subtracted from the signal to obtain the measured photon counts. This could be determined at the individual pixel level or aggregated to provide a measurement of the total photon counts

for the array. This process was repeated for each f-number at a given wavelength, in each case using the same laser power levels. The optical system exhibited a linear relationship between aperture area and count rate across the measured range (from f/2 to f/22) and at different wavelengths (600, 700, and 808 nm), as shown in Fig. 6.

From Fig. 6, it can also be observed that the magnitude of the total photon counts for the array varied depending on the wavelength, due to different optical power levels available at the three discrete wavelengths studied, and the varying detector efficiencies at these wavelengths [23]. It is clear that as the f-number was increased by one-stop, the light intensity (or total photon counts) was halved from the previous stop at any given wavelength. This linear relationship was demonstrated at three different wavelengths, 600 nm (shown in black in Fig. 6), 700 nm (red), and 808 nm (blue), respectively. In addition, these measurements also demonstrated the robustness of our optical system even at highest f-numbers, where the linear relationship between total counts (signal minus background) vs. aperture area was still satisfied (as shown from the inset in Fig. 6).

5. Results

To evaluate the performance of infinite and finite conjugate diffractive microlenses resulting from the integration on the 32 × 32 SPAD array, the concentration factor used previously in [19] was applied:

$$CF = \frac{E_0}{E_i} \tag{2}$$

where E_i is the input irradiance (optical power per unit area) at the microlens surface, and E_0 is the output irradiance or the irradiance at the photosensitive area of the pixel.

Empirically, the average concentration factor is the ratio of the total photon counts over the entire SPAD array, with and without microlenses, under the same illumination conditions. As described above, this takes into account a background subtraction stage. Hence, the average concentration factor at a given f-number was the result of two measurements which were performed for each sensor, with and without microlenses, one illuminated (at a specific wavelength) and the other under dark conditions. Each measurement consisted of 10 frames (with a frame duration of 130 ms) which were acquired, and the counts for each pixel of the SPAD array in each frame were summed. Before calculating the CF, hot-pixels were removed from both the detected photon profile measured for both SPAD arrays, with and without microlenses, by using a median filter of rank 3 × 3. In this case, hot-pixels were defined as those SPADs within the array with a DCR more than 2.5 times higher than the average DCR. The number of resulting hot pixels (with and without microlenses) was less than 5% of the total pixels in each of the SPAD arrays used in these measurements.

Figure 7 shows the average CF measured for the SPAD array with integrated infinite conjugate diffractive microlenses, as a function of the f-number (between f/2 and f/22 with one-stop increment) measured at seven discrete wavelengths between 500 and 900 nm.
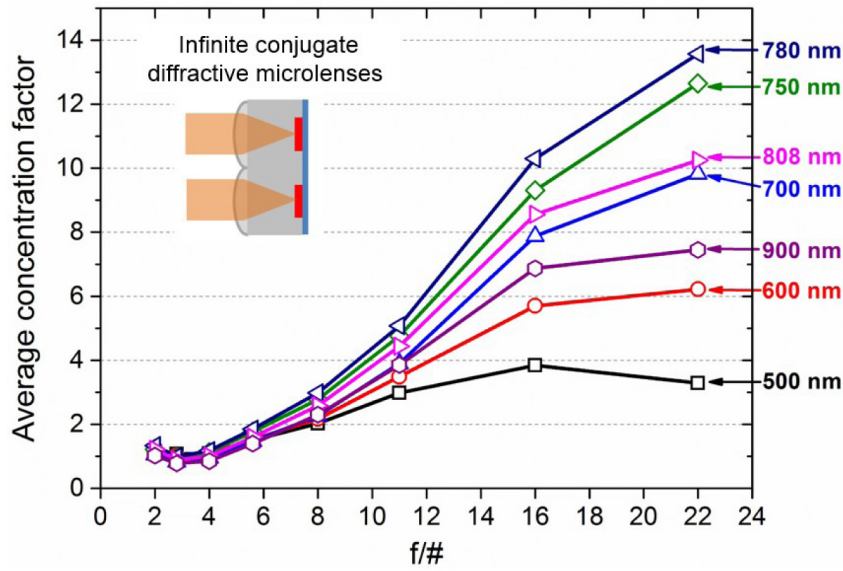
Fig. 7. Measured average concentration factor for the SPAD array integrated with infinite conjugate diffractive microlenses, as a function of the f-number (from f/2 to f/22 with one-stop increment). The measurements were performed at seven discrete wavelengths in the range 500 nm to 900 nm.

Although the infinite conjugate microlenses were designed for a wavelength of 808 nm, these showed an average concentration factor of greater than unity across the whole wavelength range under investigation (500 – 900 nm), as shown in Fig. 7. In particular, the highest average CF of ~14 was measured at λ = 780 nm and at the largest f-number of f/22. At the design wavelength (808 nm) the average CF was lower (but still high) and reached a maximum value of ~10 at f/22. The observed wavelength shift, from 808 nm to 780 nm is most likely due to tolerance errors during the microlens array fabrication. In Fig. 7, a small decrease in average CF is found when increasing the f-number from f/2 to f/2.8, and we believe that this is likely due to a small cross-talk contribution from adjacent microlenses that will not occur at larger f-numbers.

The shift of maximum efficiency from the design wavelength is also evident in the measurements of CF for the SPAD array integrated with the finite conjugate diffractive microlenses, as shown in Fig. 8. Further investigation is ongoing in order to better understand and evaluate this issue. In the case of the finite conjugate microlens array, the highest CF of 15 was measured at the peak wavelength of 750 nm and f/16, while it was lower and equal to ~7 at the design wavelength of 808 nm and f/16.
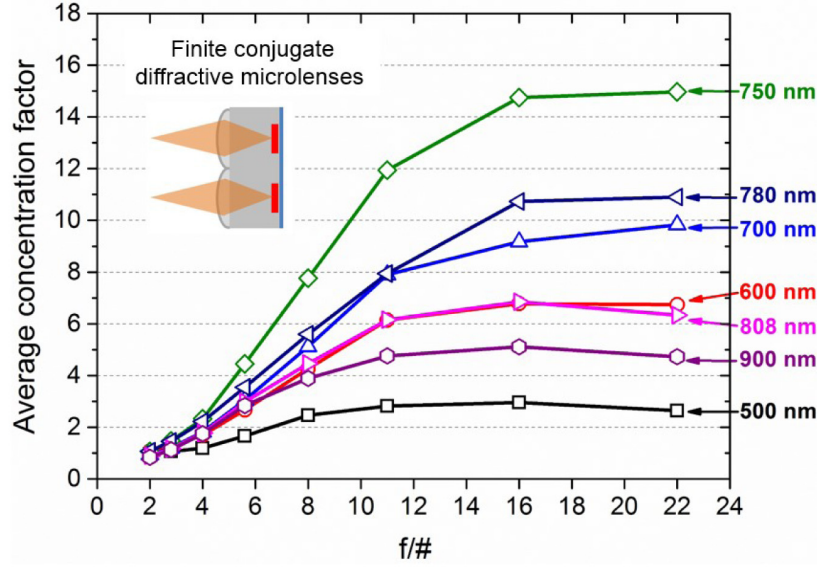
Fig. 8. Measured average concentration factor for the SPAD array integrated with finite conjugate diffractive microlenses, as a function of the f-number (from f/2 to f/22 with one-stop increment). The measurements were performed at seven discrete wavelengths in the range 500 nm to 900 nm.

It is evident from Fig. 7 and Fig. 8 that the average CF increased as the f-number was increased for both sets of microlens arrays, reaching the highest values at the largest f-numbers. At low f-numbers between f/2 and f/5.6, the aperture stop diameter is relatively large and the light coming out from the double telecentric imaging system has a large cone angle (e.g. at f/4, the cone angle ~14°), while at higher f-number the aperture diameter is smaller and, therefore, the light cone angle is considerably reduced (e.g. at f/16 is ~3.57°). Simply due to etendue conservation, it is not possible for the low f-number illumination to operate as effectively as high f-number illumination. As a consequence, at low f-number the microlens arrays cannot concentrate the light on to the SPAD active areas as efficiently as they do at the higher f-numbers. The expected saturation of the concentration factor is observed at f-numbers greater than f/16 in the case of the finite conjugate configuration.

It can be observed from Fig. 7 and Fig. 8 that the behavior of both microlenses can be divided in two main groups depending on the f-number illumination: low f-number operation (between f/2 and f/8) and high f-number operation (between f/16 and f/22). In the low f-number range, the finite conjugate microlenses (Fig. 8) demonstrated a higher CF than the infinite conjugate microlenses (Fig. 7) across the entire spectral range under investigation. At high f-numbers, the CF of the SPAD array integrated with finite conjugate microlenses (Fig. 8) reached its maximum value at f/16 and, then it remained fairly constant at f/22. In contrast, the infinite conjugate microlens case (Fig. 7) continued to increase over the measured range of f-numbers up to the highest f-number (f/22). This behaviour can be explained by the aperture being very small in this f-number range, hence the light is exiting the double telecentric imaging system with a very small cone angle, approaching the situation of an object at infinity. These results also suggest that the CF of the infinite conjugate microlenses may further increase at higher f-numbers than f/22. However, this could not be easily demonstrated, due to measurement inaccuracies at the low powers available in these experiments at the small aperture settings.

The highest CF in these measurements was 15 for the finite conjugate case and 13.8 for the infinite conjugate case. The difference between the experimentally determined value of CF for the infinite conjugate microlens example and the theoretical maximum shown in Fig. 2

of 27.9, is likely due to errors in the focal positions caused by fabrication errors. Other contributions include Fresnel losses at interfaces, and possible thin film interference effects at the interfaces of the lens substrate, the optical cement and the SPAD microstructure. Variations in detection efficiency across the active area of the detector may also make a contribution to a reduced concentration factor.

Operation at low f-numbers is one of the prime objectives of this work, as this enables wider opportunities for use of SPAD arrays in applications where the detector arrays could be used in conjunction with a small f-number objective lens (i.e. f/2-f/6), for example in camera systems. Other examples of likely applications may include optical microscopy, where the detector plane will see a magnified image of the sample, and hence the detector plane must be capable of efficient operation at higher f-numbers depending on the overall level of magnification required, but typically in the range f/8-f/32. The issue of spectral coverage is also important, however in many applications only a restricted range of wavelength is required. For example, in active imaging, or in fluorescence decay analysis, a narrow, pre-determined wavelength coverage is likely to be used.

In the examples shown, the use of finite conjugate microlenses led to improved operation at lower f-numbers. This may be partly due to the lower f-number microlens used. The infinite conjugate microlens array will provide diffraction-limited performance for collimated light, however as the f-number decreases, the lens will effectively become increasingly defocussed in the defined detector plane.

The spatial uniformity of the SPAD arrays was measured, in order to ascertain the effect of integration of the microlens arrays. We evaluated detection non-uniformity in terms of the Coefficient of Variation (CV) which is defined as the ratio of the standard deviation (σ) and the mean (μ) of the number of detected photon across the array. Figures 9(a) and 9(b) show results obtained for all three SPAD arrays (bare chip, infinite and finite conjugate microlenses) at the design wavelength (808 nm) and using f/16 illumination. All measurements in Fig. 9(a) were taken under the same illumination conditions.
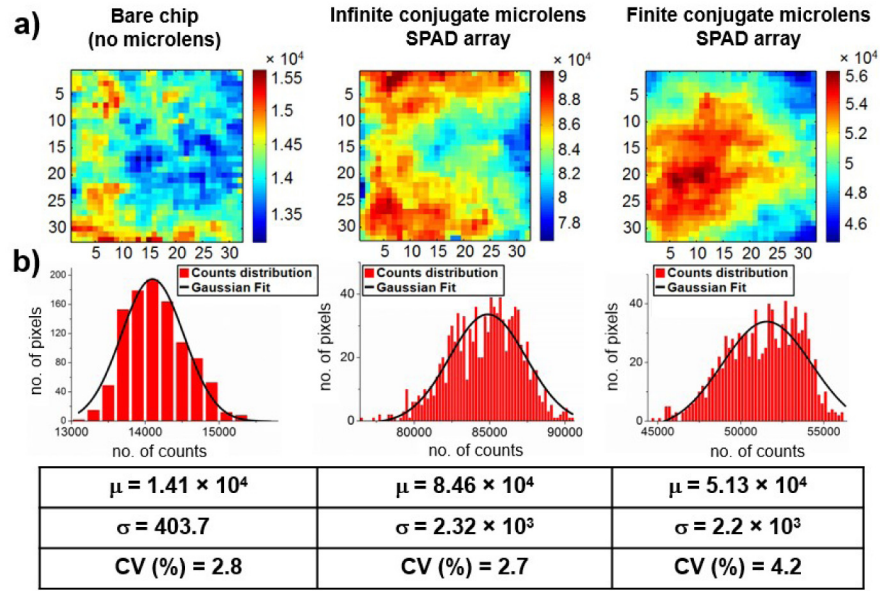

Fig. 9. (a) Photon event profile and (b) photon counts (or light intensity) distribution with the Gaussian fit for all three SPAD arrays. On the left is the bare chip (without microlenses). The middle column shows the infinite conjugate microlens SPAD array. The right-hand column shows the finite conjugate microlens SPAD array. All the measurements were acquired using f/16 illumination at the design wavelength (808 nm). The hot pixels were removed from the image by using a median filter. The value of mean (μ), standard deviation (σ), and coefficient of variation are reported in the table for each of the three detector arrays. .

A CV of 2.8%, 2.7% and 4.2% was observed for the SPAD array without microlenses (bare chip), with infinite conjugate microlens array and with finite conjugate microlens array, respectively, using f/16 illumination and at the design wavelength (808 nm). As in the case of the CF, the uniformity of all three SPAD arrays was measured at various f-numbers and three different wavelengths. Figure 10 illustrates the uniformity for all three SPAD arrays at the design wavelength of 808 nm. In general, all three SPAD arrays demonstrated good uniformity, since the variation of the light intensity across the chip was less than 6% at all f-numbers and at the design wavelength. Additionally, a variation of the light intensity for all three SPAD arrays of less than 6% was also measured at different wavelengths other than the design wavelength.

These results demonstrated that microlens integration did not introduce any measurable degradation of the uniformity of the SPAD array. In addition, the robustness of the optical setup used for the array characterization was further confirmed since the CV only slightly varied in the f-number range between f/2 and f/22.
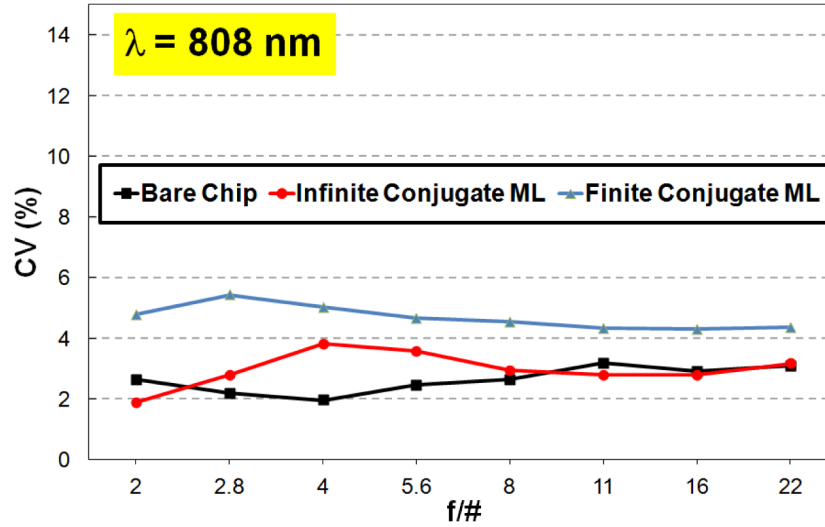

Fig. 10. Spatial uniformity of detection measured as the Coefficient of Variation (CV) as a function of the f-number (from f/2 to f/22 with one-stop increment) at the design wavelength (808 nm) for the bare chip (black), the infinite (red) and finite (light blue) conjugate diffractive microlens arrays.

6. Conclusions

We have reported the design, integration and characterization of diffractive microlens arrays onto a 32 × 32 CMOS SPAD detector array. Prior to microlens integration, the fill-factor of the bare CMOS SPAD array was 3.14%, and after the integration of microlenses the improvement of the fill-factor was analyzed over a range of wavelengths (500 – 900 nm) and a range of f-numbers (f/2 to f/22). The microlens arrays were designed in both infinite and finite conjugate configurations. The fill-factor improved at all f-numbers and wavelengths investigated, and we measured a maximum concentration factor of ~15 averaged over an entire SPAD array using an integrated diffractive microlens array. The SPAD arrays, with and without microlenses, were evaluated in terms of the spatial uniformity of detection efficiency, and a variation between 2% and 6% was measured at different f-numbers. These results demonstrated that the integration of the microlens arrays did not significantly impact the detection uniformity, illustrating negligible systematic errors in both the fabrication and integration process. Whilst these results indicate a clear route forward for improvement of SPAD fill-factor, the challenge is to increase the concentration factor at low f-number

operation. To achieve this, designs of diffractive microlenses are being investigated using a larger number of phase levels and reducing the minimum feature size to increase the coupling efficiency. Improved fabrication processes will improve the tolerance limits on the focal lengths of the microlens arrays, and the use of anti-reflection coatings can also help increase concentration factors. In addition, thinner substrates will be used in future work to decrease the microlens f-numbers, by adapting the fabrication processes accordingly. Infinite conjugate configuration microlens arrays on thinner substrates is the most obvious route forward, as preliminary analysis confirms the expected higher levels of crosstalk in the finite conjugate configuration microlenses on similar substrates. In addition, the same integration techniques has already been investigated with high sag refractive microlens arrays which can, in principle, also permit low-f number operation. However, refractive microlenses have potential issues with yield, reproducibility and the incomplete coverage of the square pixel area with the commonly used resist-reflow technique. All of these issues have been shown to be less challenging when using the diffractive microlens approach.

Acknowledgments